





## Article

# Detailed Energy Analysis of a Sheet-Metal-Forming Press from Electrical Measurements

Camilo Carrillo <sup>1,\*</sup> , Eloy Díaz Dorado <sup>1</sup> , José Cidrás Pidre <sup>1</sup>, Julio Garrido Campos <sup>1</sup> ,  
Diego San Facundo López <sup>1</sup> , Luiz A. Lisboa Cardoso <sup>1</sup> , Cristina I. Martínez Castañeda <sup>2</sup>  
and José F. Sánchez Rúa <sup>2</sup>

<sup>1</sup> Research Group on Efficient and Digital Engineering, University of Vigo, 36310 Vigo, Spain; ediaz@uvigo.es (E.D.D.); jcidras@uvigo.es (J.C.P.); jgarri@uvigo.es (J.G.C.); diego.sanfacundo@uvigo.es (D.S.F.L.); lisboa.cardoso@ieee.org (L.A.L.C.)

<sup>2</sup> Stellantis Group, 36210 Vigo, Spain

\* Correspondence: carrillo@uvigo.es

**Abstract:** This paper presents a methodology that allows for the detection of the state of a sheet-metal-forming press, the parts being produced, their cadence, and the energy demand for each unit produced. For this purpose, only electrical measurements are used. The proposed analysis is conducted at the level of the press subsystems: main motor, transfer module, cushion, and auxiliary systems, and is intended to count, classify, and monitor the production of pressed parts. The power data are collected every 20 ms and show cyclic behavior, which is the basis for the presented methodology. A neural network (NN) based on heuristic rules is developed to estimate the press states. Then, the production period is determined from the power data using a least squares method to obtain normalized harmonic coefficients. These are the basis for a second NN dedicated to identifying the parts in production. The global error in estimating the parts being produced is under 1%. The resulting information could be handy in determining relevant information regarding the press behavior, such as energy per part, which is necessary in order to evaluate the energy performance of the press under different production conditions.

**Keywords:** industrial machines; energy patterns; nonintrusive load monitoring; artificial neural networks; part classification



**Citation:** Carrillo, C.; Díaz Dorado, E.; Cidrás Pidre, J.; Garrido Campos, J.; San Facundo López, D.; Lisboa Cardoso, L.A.; Martínez Castañeda, C.I.; Sánchez Rúa, J.F. Detailed Energy Analysis of a Sheet-Metal-Forming Press from Electrical Measurements. *Energies* **2023**, *16*, 6972. <https://doi.org/10.3390/en16196972>

Academic Editors: Inga Konstantinavičiute, Viktorija Bobinaite, Vaclovas Miškinis, Saulius Gudžius and Daiva Dumciuvienė

Received: 11 September 2023

Revised: 3 October 2023

Accepted: 4 October 2023

Published: 6 October 2023



**Copyright:** © 2023 by the authors. Licensee MDPI, Basel, Switzerland. This article is an open access article distributed under the terms and conditions of the Creative Commons Attribution (CC BY) license (<https://creativecommons.org/licenses/by/4.0/>).

## 1. Introduction

The technique of non-intrusive load monitoring (NILM) has long been used for the identification, diagnosis, and event prediction of industrial machines since the term was explicitly coined in the 1980s in the context of residential and commercial environments [1].

The principle involved in NILM is that all activity ongoing on a machine or industrial appliance correlates with the mechanical and electrical signals that can be measured either within or externally to this machine. Sometimes, it is not possible, or not as easy, to monitor variables that are only internally available, which could characterize the state of the machine in better detail [2]. However, the externally accessible signals, consisting, for instance, of the instantaneous power being supplied to different modules of an industrial machine, often convey enough information about the machine's activity [3–5]. This allows for system analysis and identification, as represented in Figure 1. In addition, electric power signals are easy to monitor externally using commercial monitoring equipment, which implies the faster deployment of a data collection system.

Popular NILM objectives are load disaggregation and activity identification [6–9]. In load disaggregation, the target is to identify the specific power consumption of each machine among a group of devices that can be turned on or off individually. This immediately leads to knowing whether any discrepancy is being observed in the energy consumption pattern of each machine, either due to a transient or a long-term condition, allowing the

generation of warnings for the final electricity user [10]. Load disaggregation is a complex task that can be solved by different approaches as an optimization problem [11,12]. Extensive use of load disaggregation techniques has been reported to support better energy management, demonstrating the potential of this technique to provide energy demand forecast and an overall reduction in energy consumption [13].

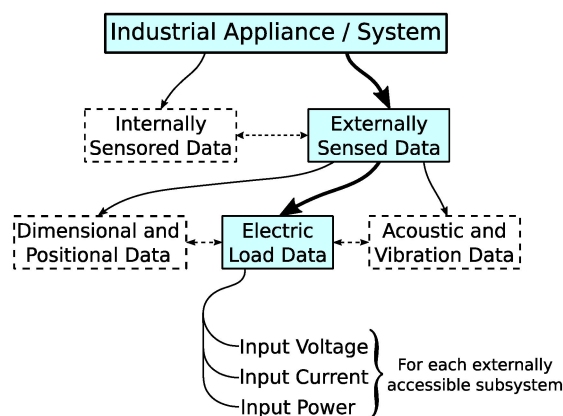


**Figure 1.** NILM: Externally monitorable variable electric data.

The detailed analysis of the isolated power signals of individual machines can additionally provide more information on the specific activity being carried out by those machines [5]. Typically, this has been applied to residential installations to build consumer models at the residential level [14], but the strategy has been used to monitor and analyze industrial activities as well, for example, with the aid of big data [15], artificial intelligence [16], or by using hidden Markov models [17].

As mentioned in the previous section, there are few NILM methods used for industrial applications, and most of them are intended to perform an energy analysis of the processes involved [3–5,18,19]. Nevertheless, activity identification can be seen as a complementary objective when knowledge of the outcome production of a machine is desired. Such objectives are easier to achieve when some degree of machine subprocess disaggregation is possible. Large machines are usually powered by multiple power lines that are individually accessible in external electrical boxes, allowing for the aforementioned disaggregation.

In this context, this paper presents a methodology that allows us to detect the state of a metal stamping transfer press, the parts under production, their cadence, and the energy demand for each unit produced. For this purpose, only electrical measurements are used, taking advantage of the fact that a machine is supplied by different power lines for different sub-processes.

The machine analyzed in this paper is a transfer press, which is described in Section 2. Section 3 presents the measurement setup and its characteristics. In Section 4, methods for the detection of the states of the press and the detection of the part being produced are presented. The performance of these methods is analyzed in Section 5. Finally, the conclusions which were derived are summarized in Section 6.

## 2. The Sheet-Metal-Forming Transfer Press

Commonly referred to as transfer press, the sheet metal transfer press machines are some of the largest machines used in the automotive industry and produce an assorted number of component parts necessary for vehicle assembly [20]. These machines ordinarily operate in a very high-duty cycle, thus requiring large amounts of energy for their activity. Because of this, the forming processes have already been the subject of comprehensive studies concerning energy conservation [21]. These machines operate in a cyclic pattern, producing sequences of hundreds of samples of the same part on each run. From time to time, production is momentarily stopped and these presses are reprogrammed to produce

new required parts. Eventually, an unexpected condition may occur, and production must be interrupted in order to clear or reset the machine.

The machine analyzed in this study is several meters long, weighs about 1200 metric tons, and has a rated power of 560 kW. It works in three sequential pressing stages with its corresponding heads (see Figure 2) and bed cushions. A flywheel, driven by the main motor of the press, is responsible for maintaining the speed of the heads at a constant value. Each head has an associated pressing carriage. The pressing power of carriage 1 is 12,500 kN, with a stroke of 1.1 m, while carriages 2 and 3 perform their function at 10,000 kN, with a stroke of 1 m. On the other hand, the bed cushion has a total force between 350 kN and 3000 kN and a stroke between 20 and 250 mm.

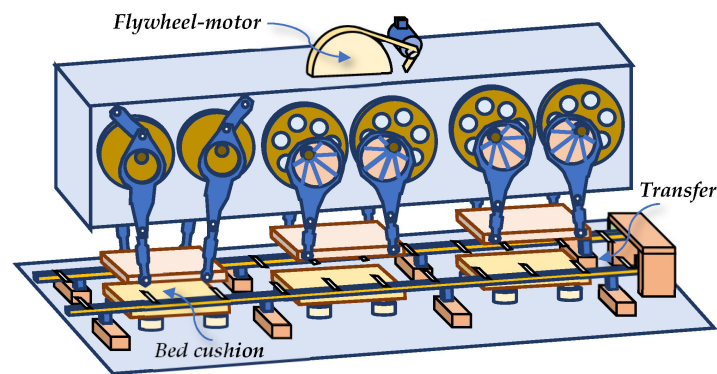


**Figure 2.** Three-dimensional simplified representation of the transfer press.

A transfer with the following actions moves the parts inside the press: forward/reverse, ascending/descending, and opening/closing.

### 3. Measurement of Electrical Parameters

Due to its high power requirements, the press power supply is divided into four power lines that feed the following subsystems (see Figure 3):

- Flywheel-motor;
- Transfer;
- Bed cushion;
- Hydraulic and other auxiliary subsystems.

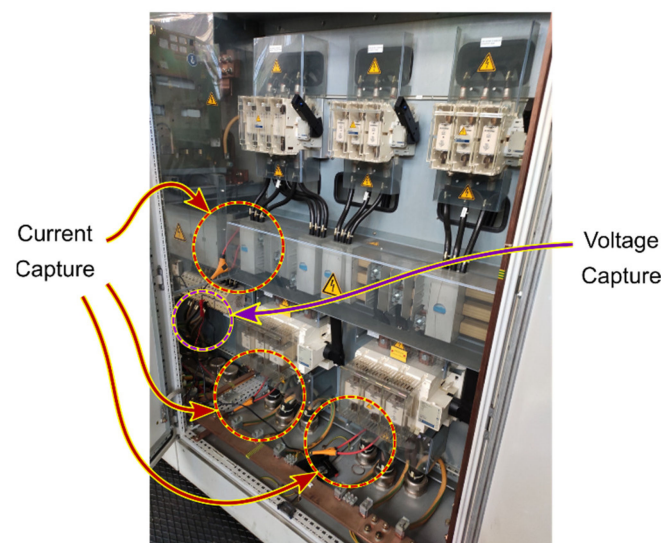


**Figure 3.** Measurement of currents and voltages at the press switchboard.

A six-month measurement campaign was conducted from 2021 to 2022 on the above circuits.

The electrical parameters were monitored using a power quality monitor that samples voltage and current at several kHz. From these values, it calculates the root mean square (RMS) and power values every 20 ms. This high sampling rate is necessary because of the dynamic nature of the transfer movements. In this situation, obtaining values at the rate recommended by international standards, e.g., every 100 ms, as specified by the International Electrotechnical Commission standards, would not allow the cyclic behavior of the transfer to be adequately detected. A low pass filter was applied to the measured signals to eliminate the high-frequency noise associated with the motor drivers.

Electric measurements have been complemented by a data file where press operators log the produced parts. This information is crucial in order to train the classifiers for part type identification.

#### 4. Feature Extraction and Classification

##### 4.1. Methodology Overview

This section presents the methodology for detecting the state of the press and identifying the part being produced. It can be summarized as shown in the diagram in Figure 4.

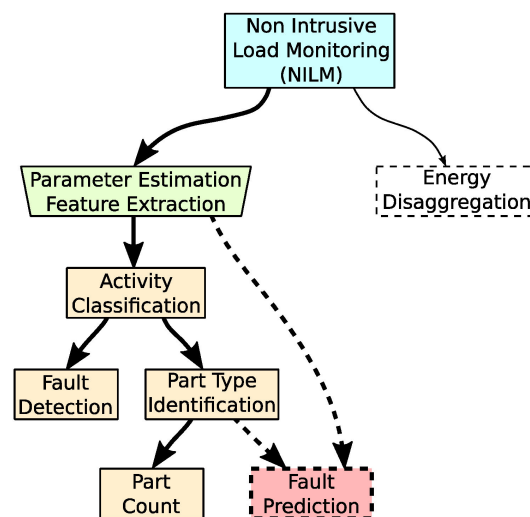


**Figure 4.** Activity classification and estimation goals.

The features to be extracted from the input power signal are selected according to the goals set for automatic analysis of the press activity, which are:

- The identification of when the press is in normal production activity and the recognition of individual press production cycles;
- The identification of the parts being produced;
- The estimation of the production rate in parts per minute;
- The estimation of the energy required to produce each part being manufactured.

While the three first information items are mostly related to productivity analysis, the final item also offers an opportunity to control the quality and assess each part's energy cost.

To accomplish these goals, the press state is initially evaluated to determine when there is ongoing normal production activity (Running state, in Figure 5). Then, for these periods, the production cycles are identified, allowing for the estimation of press cycle times and the total press energy expended in the production of each part. Based on the frequency, the part type in production is also inferred based on the observed frequency pattern of one of the power signals.

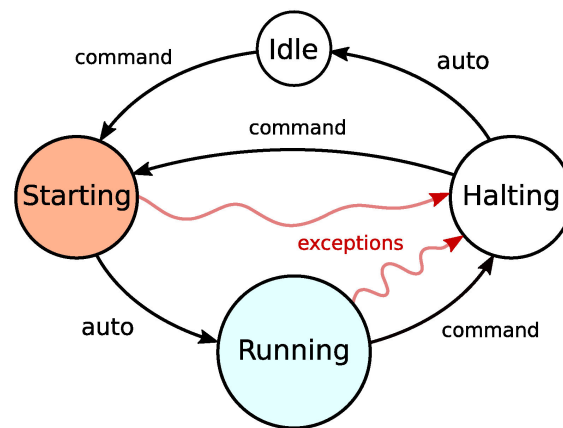


**Figure 5.** State diagram for the sheet-metal-forming press.

The NNs for estimating press states and identifying parts in production were designed using the MATLAB Neural Network Pattern Recognition tool [22].

#### 4.2. Press State Estimation

##### 4.2.1. Press States

The press states under consideration are (see Figure 6):

- **Running:** The press is running in a steady-state regimen. The power measured at the flywheel motor and transfer shows cyclical behavior.
- **Idle:** The press is powered on but not in motion. Transfer and flywheel motor consumption are both low and have very little variation.
- **Starting:** The system accelerates its movements until reaching the Running state. The flywheel motor begins to increase consumption until it undergoes a peak followed by a drop in current, then stabilizes in a steady state. The transfer consumes power in an oscillatory way, increasing the intensity peaks until it returns to the cyclic pattern.
- **Halting:** The press stops and enters the Idle state. The flywheel motor experiences an overcurrent followed by a slight oscillation until it stabilizes at a current value, at which point the press stops. The current of the transfer motor stabilizes, exhibiting almost no fluctuation.

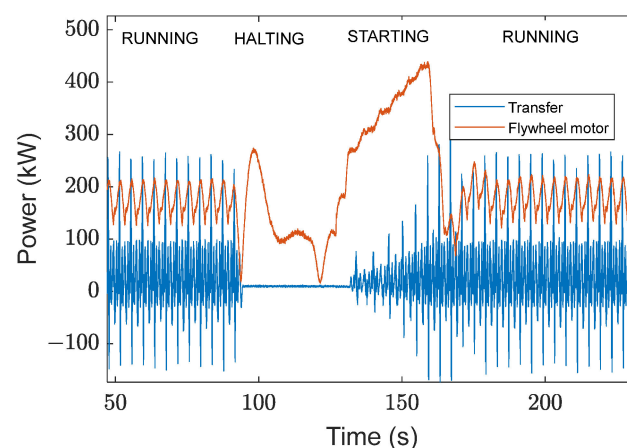


**Figure 6.** Typical motor and transfer power signal evolution as the press evolves through non-idle states.

The transitions between the states are represented in Figure 5, where it can be seen that, in some circumstances, the press can enter the Halting state due to safety directives or fault conditions.

#### 4.2.2. Idle State Identification

As mentioned above, one of the main characteristics of the Idle state is the stability of the power consumed by the flywheel and the transfer. To establish when the press is in this state, histograms of the standard deviation of RMS currents in these elements have been analyzed (see Figure 7). As a conclusion, limits for those deviations have been established (17 A for the transfer and 4 A for the flywheel motor) so that the Idle state is fully identified.

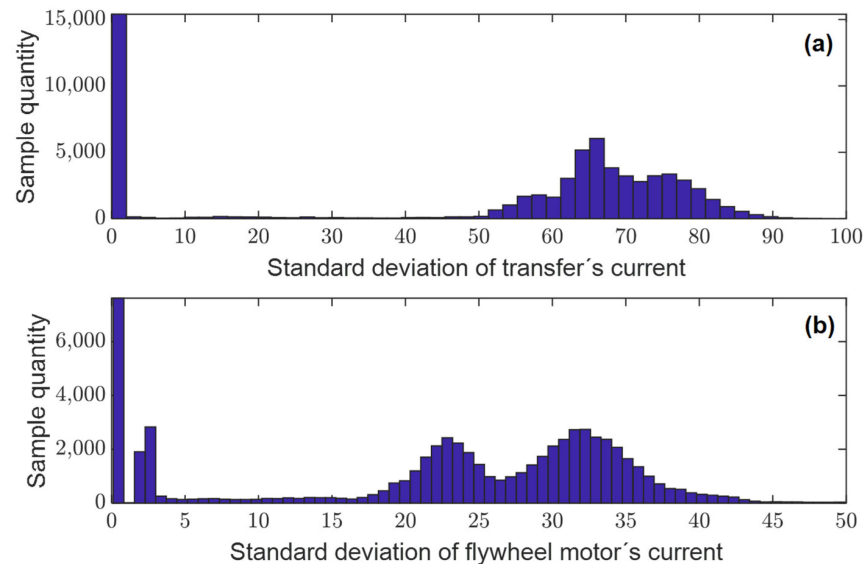


**Figure 7.** Histograms of the standard deviations of the current intensities in the last 5 s (previous 250 points measured) for all recorded data: (a) of the transfer module and (b) of the flywheel motor.

#### 4.2.3. Starting, Halting, and Running State Identification

The evolution of the current and power during the Starting and Halting states is quite complex. To determine whether the press is in one of these states, it is necessary to analyze both the current and previous values.

After a detailed analysis of the current and power evolution during those estates, the variable selected to analyze them is the mean value of the RMS current over a moving window of 10 s. It can be denoted as follows:

$$I_{ti}^{sys}, \quad (1)$$

where super index *sys* identifies the system whose current is being analyzed (*tr*: transfer; *fm*: flywheel motor), and *ti* refers to the window where the average current is calculated (e.g., *ti* = 20–30 refers to the windows between 20 s and 30 s before the instant being analyzed).

A neural network (NN) for classification [23], the characteristics of which are shown in Table 1, was used to detect the press states. This NN has 12 inputs, which are summarized in Table 2. An example of the temporal sequence of these inputs is shown in Figure 8, where it can be seen that mean current values from the previous 60 s are necessary to identify the pressure state.

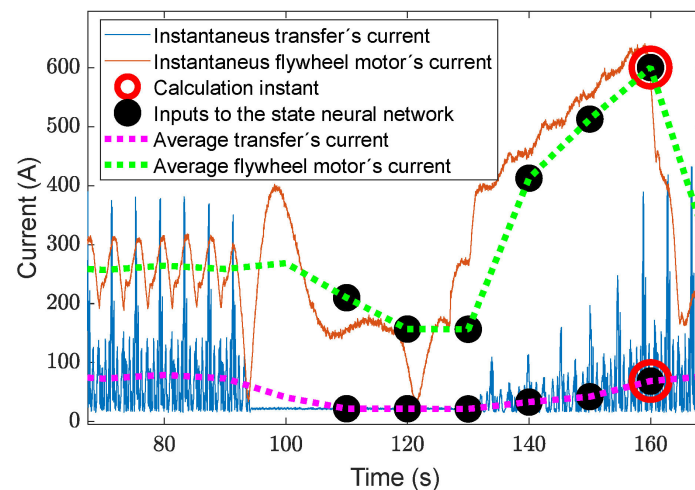
**Table 1.** Characteristics of state identification NN.

Type	Classification
No. of layers	2
Hidden neurons	sigmoid
No. neurons in the hidden layer	50
Output neurons	softmax
Training	SCG backpropagation



**Table 2.** State identification NN's inputs.

Input no.	Subsystem	Interval		Variable
		Start	End	
1	Transfer	10 s	0 s	$I_{0-10}^{tr}$
2		20 s	10 s	$I_{10-20}^{tr}$
3		30 s	20 s	$I_{20-30}^{tr}$
4		40 s	30 s	$I_{30-40}^{tr}$
5		50 s	40 s	$I_{40-50}^{tr}$
6		60 s	50 s	$I_{50-60}^{tr}$
7	Flywheel motor	10 s	0 s	$I_{0-10}^{fm}$
8		20 s	10 s	$I_{10-20}^{fm}$
9		30 s	20 s	$I_{20-30}^{fm}$
10		40 s	30 s	$I_{30-40}^{fm}$
11		50 s	40 s	$I_{40-50}^{fm}$
12		60 s	50 s	$I_{50-60}^{fm}$

**Figure 8.** Sequence of inputs for the state identification NN.

NN architecture for press state identification is shown in Figure 9. For the initial training, the machine states were classified heuristically by analyzing the trends of the currents between the steady state production (Running) and the machine stop (Idle). The data set comprised 22,000 values, and was divided into:

- Training: 70%
- Validation: 15%
- Test: 15%

Additionally, a threshold was established in the resulting discrete probability density given by NN. This avoids misclassification, because the training is based on heuristic rules. Thus, outputs are valid only if their probability exceeds the established threshold. No valid outputs are associated with an Unknown state. The established probability thresholds are:

- For Running: 0.8
- For Starting and Halting: 0.7

The press state estimation provides general insight into the activity being performed by the press; in particular, the press state signalizes when normal production cycles are

expected (Running state), and the part type inference can conveniently be made. During the observation period of this study, the press was only in the idle state about 17% of the time and in normal production about 73% of the time, as shown in Table 3.

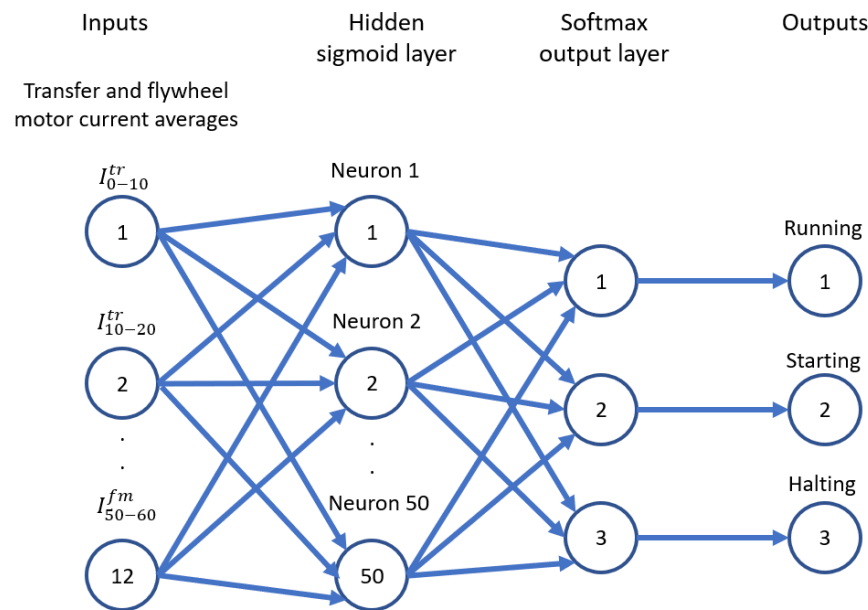


Figure 9. NN architecture for press state identification.

Table 3. Press activity statistics.

Press State	Number of Observed Intervals	% of Time
Running	34,873	73.2%
Starting	2552	5.4%
Halting	1883	4.0%
Idle	8179	17.2%
Unknown	138	0.3%
Total	47,633	100%

#### 4.3. Press Cycle Period Estimation

##### 4.3.1. Periodic Behavior with Power Signals

When the press is in normal operation, i.e., producing parts, a periodic pattern can be observed in the power consumed by the flywheel motor and the transfer. That makes it natural to use harmonic coefficients to solve the problem of part type identification. This approach is similar to that used to analyze vibrations and rotative machines in general [24,25] and in some NILM methods [26]. The intuitive reasoning behind this approach is that the relative magnitude of the harmonic coefficients relates directly to the movements of the transfer and the specific geometry of the part being produced. When calculated over an integer number of press cycles, these coefficients are expected to be insensitive to a particular production rate during normal press operation. This makes obtaining the production period from the power signals necessary before conducting the Fourier analysis.

In practice, the press works continually, producing parts of the same type for long periods, as is required by the production schedule, and all cycles in the same batch have the same characteristics. Thus, because long time intervals can be observed with all cycles corresponding to the production of the same part type, several identical cycles can be used to obtain the harmonics, increasing the accuracy of the results.



By inspection (see Figure 10), it was verified that during normal production activity, the power input to the bed cushion module and the hydraulic and auxiliary subsystems of the press is approximately constant and does not convey substantial information on the parts being produced. On the other hand, both the flywheel motor and transfer power demand become periodic, reflecting press movements and mechanical efforts, cycling according to the press-forming pace. In particular, the input power to the flywheel motor is entirely dominated by the component at the first harmonic (the fundamental press frequency), as shown in Figure 10.

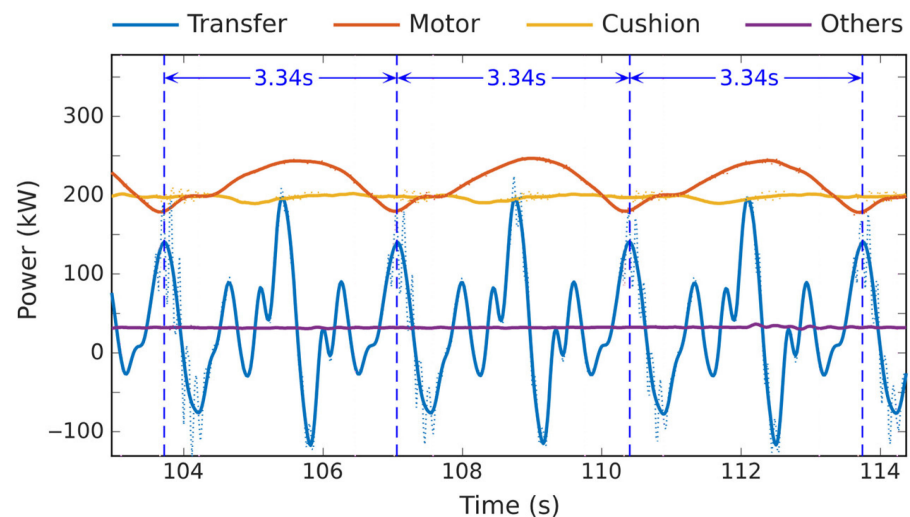


**Figure 10.** Power values of the different press subsystems when producing parts of type #11.

This behavior was observed for all types of parts, although the detailed shape of the power signal may have differed for different parts. The production cycle can approximately be associated with the interval between two consecutive relative maximum and minimum points in the power consumed by the flywheel motor or transfer.

#### 4.3.2. Press Cycle Period Estimation and Harmonic Analysis

Since the transfer power and the flywheel motor power show periodic behavior, both can be used to detect the duration of the production cycle (see Figure 10). The transfer power signal was chosen as the most suitable option for this purpose because of its sharper shape, which allows for a more precise period to be obtained.

The production period ( $T_{prod}$ ) is obtained from the transfer power signal using the least squares Levenberg–Marquardt algorithm for the harmonic decomposition expression [27]. This analysis is performed on a 30 s moving window to obtain sufficient cycles (typ.  $\geq 5$ ) in order to accurately estimate the period.

##### Inference of Part Type Being Produced

A strong regularity was observed in the frequency pattern of the periodic power signal of the transfer module during the normal production of each part of the same type (see Figure 10). This motivated the use of the Fourier coefficients of this signal as a feature space for part type inference during steady-state production (Running state). The power signal was resampled using an interpolation method to increase the accuracy of the results [28].

Initially, to explore the adequacy of the separation of part classes in the frequency domain, the scattering of all the Fourier coefficients of the transfer power signal in 30 s intervals with the press in the running state was plotted. It showed that a good separation of the part classes could be established. This could be achieved, for instance, by either using the 1st and 7th coefficients or the 3rd and 8th harmonic coefficients normalized to the largest of these coefficients, as shown in Figure 11.

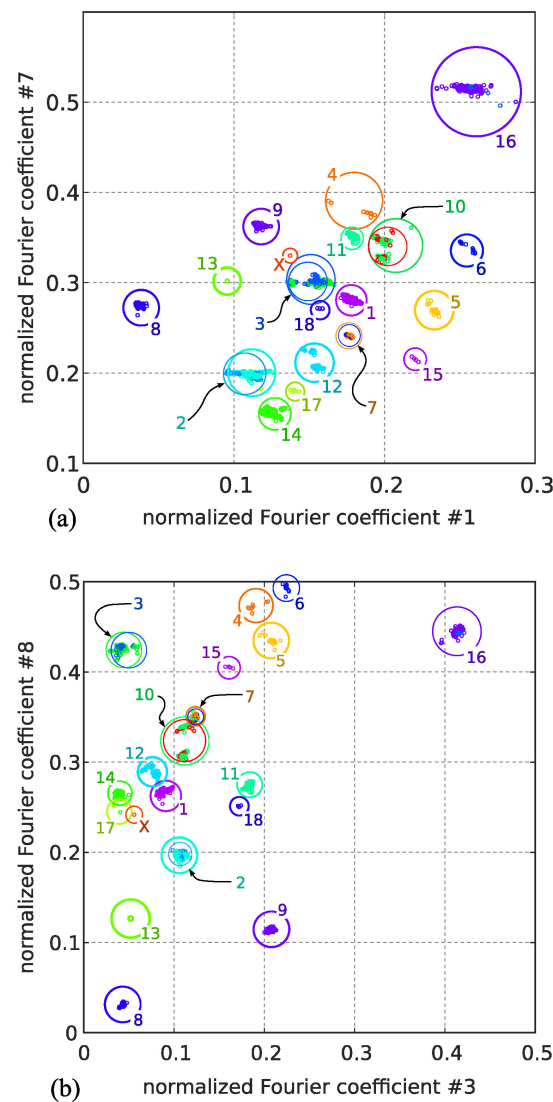


**Figure 11.** Scattering of parts based on normalized Fourier coefficients of the transfer power signal results with good separation of the part types (see numbers 1 to 18): (a) using 1st and 7th coefficients; (b) using 3rd and 8th coefficients.

Visual separation of the part classes was easily obtained by this method, except for symmetric parts, such as “left door” and “right door”, which were indistinguishable. In this approach to the classification problem, these twin parts were then fused into single-part classes #2, #3, #7, and #10, as indicated in Figure 11 by arrows.

The group marked with an “X” represents a subclass with only a single record available, and due to this lack of sufficient information, this class was excluded from the posterior analysis.

This examination of the available data confirmed the adoption of normalized Fourier coefficients as a good feature space for classifying part types. An example of the power transfer waveforms with their normalized Fourier coefficients can be seen in Figure 12. The physical justification for this choice is that the relative magnitude of the Fourier coefficients should be independent of the fundamental frequency of the transfer power signal, i.e., the production rhythm, regardless of the part class being produced. The relative Fourier coefficients are associated with the motion pattern of the transfer, which is expected to be directly related to the physical press actions of each part type.

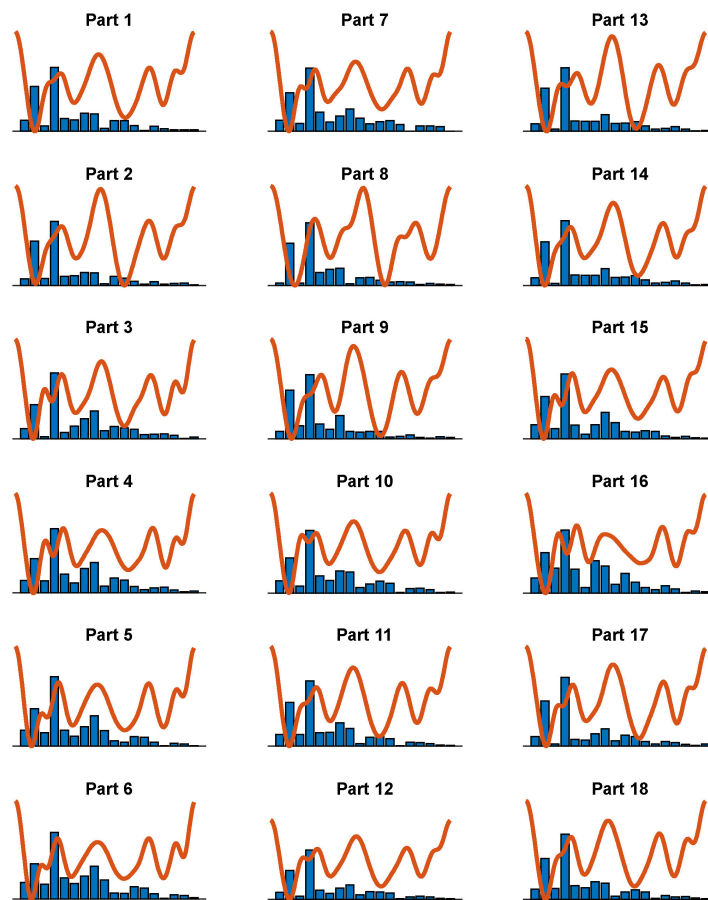


**Figure 12.** Transfer power signal (red) and its eighteen first normalized Fourier coefficients (blue) for a cycle of the parts under study.

The procedure to obtain harmonic components is summarized in Figure 13, which shows the DC component ( $a_0$ ), module, and phase of harmonics ( $c_k, \varphi_k$ ) of the transfer power signal every 10 s, with the signal sampled at 50 Hz during the previous  $N$  cycles. The total number of non-DC coefficients,  $K$ , was set at 18 because no significant energy was found in the samples of the transfer power signal above the 18th harmonic for all considered part types.

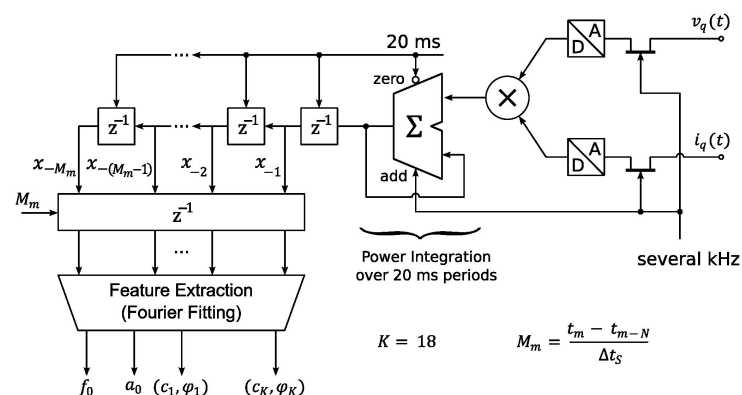


**Figure 13.** Simplified block of data collection and feature extraction.

However, to further improve the separation of the part classes and to be able to better accommodate any future introduction of new part types in the production portfolio, a feed-forward NN was trained for accomplishing the classification task, and its whose

structure can be seen in Figure 14. Its characteristics are the same as those of NN in Table 1, but with a different number of neurons. The data set was divided into:

- Training: 50%
- Validation: 25%
- Test: 25%

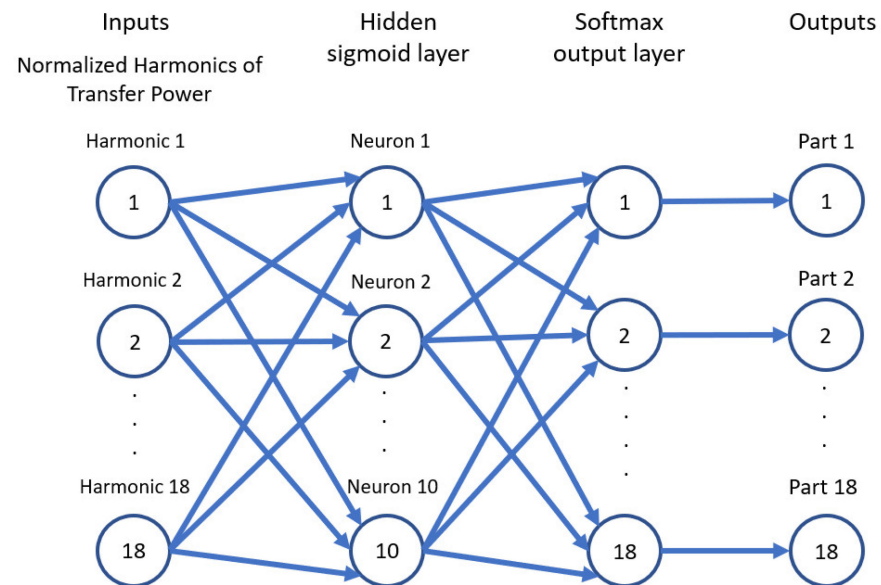


**Figure 14.** NN architecture for part type identification.

## 5. Results

The performance of the analysis system was evaluated as a function of the errors obtained during type part inference, with the ground truth established by the factory-annotated test dataset. The part inference was only assessed on signals captured when the press was in the *Running* state, as was previously computed using the press state classifier NN.

### 5.1. Press Cycle Period Estimation

As shown in Section 4.2, the production period as estimated every 10 s using a moving window of 30 s. By analyzing the result, it was found that parts can have different production rates that are constant over long periods (see Figure 15).

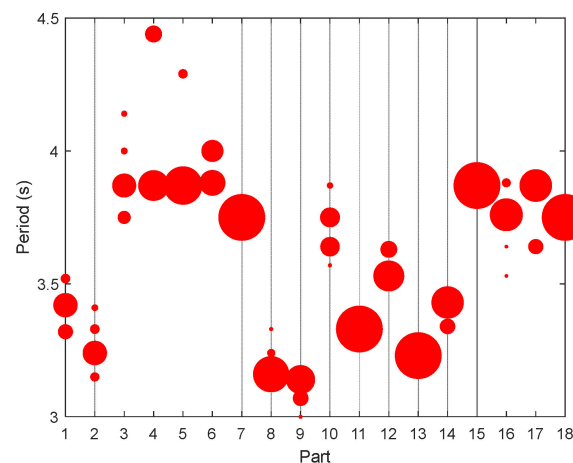


**Figure 15.** Production periods for the considered parts (the area of the circle is proportional to the percentage of the periods for each part).

### 5.2. State Estimation

The effectiveness of the resulting NN for state identification can be analyzed using the confusion matrix shown in Figure 16. It correctly detects 99.96% of the running records, 96.75% of the starting situations, and 94.73% of the halting records. It considers the remaining cases Unknown states.

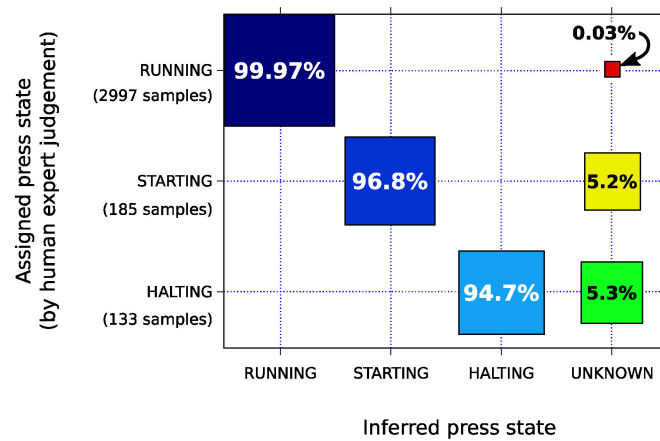


**Figure 16.** Confusion matrix for press state identification on the test data, executed after assurance that the state is not Idle.

Figure 17 shows an example of the result given by the NN on a recording not previously trained by the NN, in which the press goes from Running to Halting. It should be noted that, before the press stops completely, it returns to the Starting state and then finally to the Running state. As long as the transfer consumption is minimal, the press is considered Halting. As soon as the intensity increases, Starting is detected until it stabilizes cyclically and detects Running.

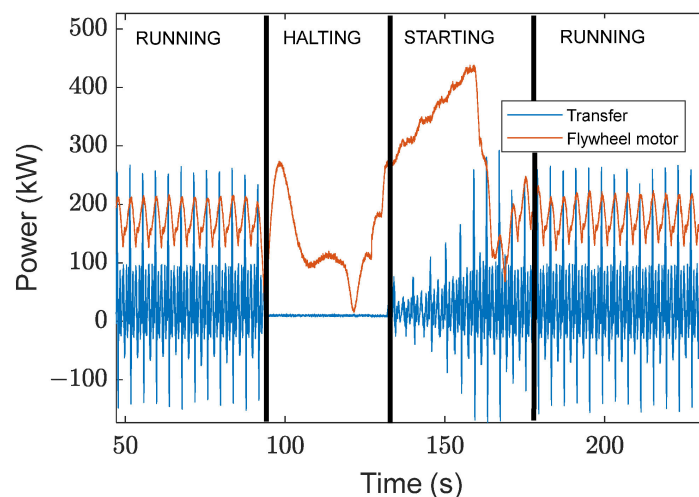


**Figure 17.** Typical evolution of transfer and flywheel motor power used to train the press state classifier, showing running, halting, and starting phases.

The resulting error can be considered relatively low since the states were initially defined by observation and heuristic rules.

### 5.3. Part Classification

The parts being produced were detected by the NN depicted in Section 4.3.2. To determine the number of neurons, the global error in detecting parts was analyzed, as shown in Figure 18. From a number of 10 neurons, the error remained stable, so this was the number of neurons chosen.

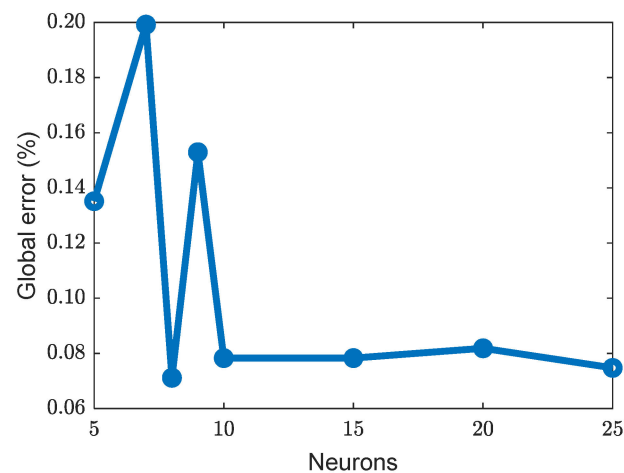


**Figure 18.** Global error in parts identification.

The confusion matrix of the part identification NN is shown in Figure 19. In this matrix, all of the 30 s Running state recordings identified by the state NN were tested, excluding all of those that were part of the training of the part NN. From a set of 18 parts, the error in 17 was between 1% and zero, while part #4 failed in 5.37% of the cases, being identified as part #11. In this case, the misclassification of part #4 was provoked by only a single record (see Figure 20), wherein the flywheel motor exhibited an unforeseen behavior that affected the harmonic content of the power transfer.

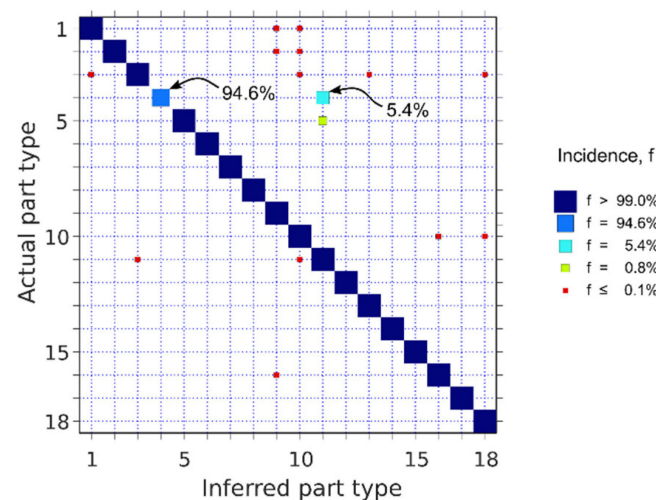


**Figure 19.** Confusion matrix of NN with ten neurons for part identification on the testing data set.

The overall success rate of the NN for classifying parts was 99.92% with untrained records, so it can be concluded that it is consistent in identifying the parts during a steady-state regime (Running state).

#### 5.4. Energy Estimation

Valuable production information can be obtained once the parts and their production rates are identified. For example, the mean energy associated with producing a single part (see Figure 21) can be estimated very accurately, because situations in which the press is not producing are not included in the calculation. Also, a detailed analysis of the impact of the production period on energy consumption is feasible, as shown in Figure 22.



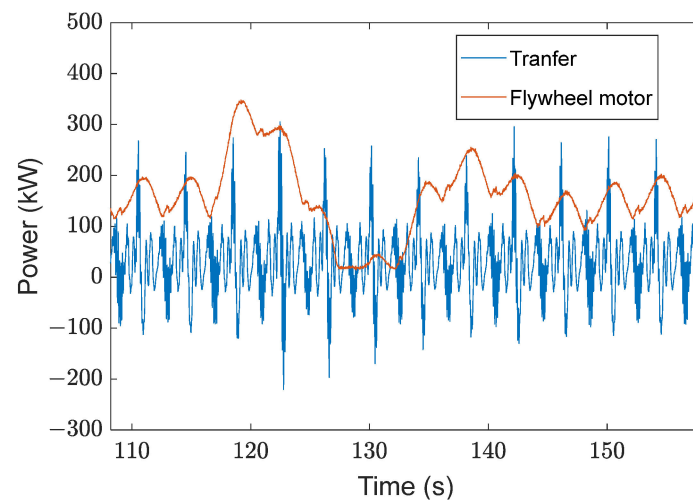


**Figure 20.** Record of the transfer and flywheel power, where part #4 is not correctly detected.

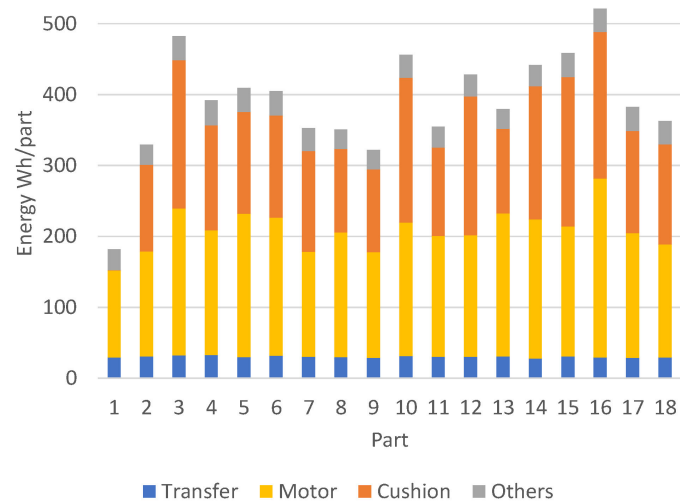


**Figure 21.** Average energy in the press subsystems during the production of the different parts.

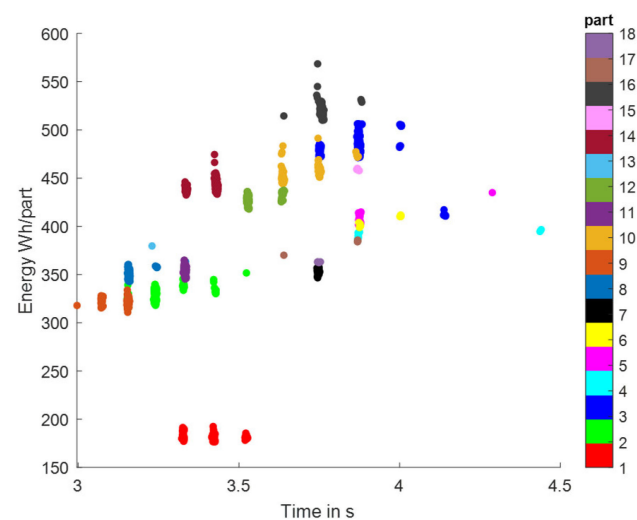


**Figure 22.** Energy consumed to produce each part versus cadence values.

## 6. Conclusions

Partially disaggregated electrical measurements collected from a sheet metal transfer-forming press were analyzed. As a result, we obtained the production rate and energy demand for every single part, as well as the part type identification. The determination of the part type was based only on the input power to the transfer module, which was obtained with a period of 20 ms.

Two neural networks (NN) were developed to detect the press state and estimate the part type under production. The first NN was based on heuristic rules for defining states and achieved a reasonably high success rate (>94%) in detecting the different press states.

Once the press states were determined, the production period or rate could be obtained during the steady-state production of the press. In order to characterize the press behavior for each part being produced, the normalized module for the 18 first harmonics was adopted. This made the characterization insensitive to the production rate.

These harmonics were used as inputs to the NN dedicated to estimating the part being produced. In this case, the global success rate was higher than 99%, and over 94% for the worst-detected part.

As a result, a methodology has been developed to detect the press state, the part being produced, and the production rate with high identification success. This information makes it possible to obtain energy ratios such as energy per part, which is a basic tool for improving the energy efficiency of a machine.

**Author Contributions:** Conceptualization, C.C., E.D.D., J.C.P. and J.G.C.; methodology, C.C., E.D.D., D.S.F.L. and L.A.L.C.; software, C.C., E.D.D., D.S.F.L. and L.A.L.C.; validation, C.C., E.D.D., C.I.M.C. and J.F.S.R.; formal analysis, C.C., E.D.D., J.C.P. and J.G.C.; investigation, C.C., E.D.D., D.S.F.L. and L.A.L.C.; data curation, C.C., E.D.D., D.S.F.L. and L.A.L.C.; writing—original draft preparation, C.C., E.D.D., J.C.P., J.G.C., D.S.F.L., L.A.L.C., C.I.M.C. and J.F.S.R.; writing—review and editing, C.C., E.D.D., J.C.P., J.G.C., D.S.F.L., L.A.L.C., C.I.M.C. and J.F.S.R.; supervision, C.C., E.D.D., C.I.M.C. and J.F.S.R.; project administration, C.C., E.D.D., C.I.M.C. and J.F.S.R. All authors have read and agreed to the published version of the manuscript.

**Funding:** This work was supported by Feder Galicia 2014–2020 (Xunta de Galicia) under Grant “FACENDO 4.0: Factory competitiveness and electromobility through innovation” (IN854A 2020/01).

**Data Availability Statement:** The data are not publicly available due to the confidential nature of the information.

**Conflicts of Interest:** The authors declare no conflict of interest.

## References

- Hart, G.W. Nonintrusive appliance load monitoring. *Proc. IEEE* **1992**, *80*, 1870–1891. [\[CrossRef\]](#)
- Herrero, J.R.; Murciego, Á.L.; Barriuso, A.L.; de la Iglesia, D.H.; González, G.V.; Rodríguez, J.M.C.; Carreira, R. Non Intrusive Load Monitoring (NILM): A State of the Art. In *Trends in Cyber-Physical Multi-Agent Systems. The PAAMS Collection, Proceedings of the 15th International Conference, PAAMS 2017, Porto, Portugal, 21–23 June 2017*; Springer: Cham, Switzerland, 2017; pp. 125–138. [\[CrossRef\]](#)
- Brillinger, M.; Wuwer, M.; Hadi, M.A.; Haas, F. Energy prediction for CNC machining with machine learning. *CIRP J. Manuf. Sci. Technol.* **2021**, *35*, 715–723. [\[CrossRef\]](#)
- Hong, H.; Zhang, C.; Meng, L.; Tian, G.; Yu, J. Characterising energy efficiency in machining processes: A milling case. In *Proceedings of the 2017 International Conference on Advanced Mechatronic Systems (ICAMEchS)*, Xiamen, China, 6–9 December 2017; pp. 83–88. [\[CrossRef\]](#)
- Hu, S.; Liu, F.; He, Y.; Hu, T. An on-line approach for energy efficiency monitoring of machine tools. *J. Clean. Prod.* **2012**, *27*, 133–140. [\[CrossRef\]](#)
- Zoha, A.; Gluhak, A.; Imran, M.A.; Rajasegarar, S. Non-Intrusive Load Monitoring Approaches for Disaggregated Energy Sensing: A Survey. *Sensors* **2012**, *12*, 16838–16866. [\[CrossRef\]](#) [\[PubMed\]](#)
- Holmegaard, E.; Kjaergaard, M.B. NILM in an Industrial Setting: A Load Characterization and Algorithm Evaluation. In *Proceedings of the 2016 IEEE International Conference on Smart Computing (SMARTCOMP)*, St. Louis, MO, USA, 18–20 May 2016; pp. 1–8. [\[CrossRef\]](#)
- Raiker, G.A.; Loganathan, U.; Agrawal, S.; Thakur, A.S.; Ashwin, K.; Barton, J.P.; Thomson, M. Energy Disaggregation Using Energy Demand Model and IoT-Based Control. *IEEE Trans. Ind. Appl.* **2021**, *57*, 1746–1754. [\[CrossRef\]](#)

9. Dash, S.; Sahoo, N. Electric energy disaggregation via non-intrusive load monitoring: A state-of-the-art systematic review. *Electr. Power Syst. Res.* **2022**, *213*, 108673. [\[CrossRef\]](#)
10. Armel, K.C.; Gupta, A.; Shrimali, G.; Albert, A. Is disaggregation the holy grail of energy efficiency? The case of electricity. *Energy Policy* **2013**, *52*, 213–234. [\[CrossRef\]](#)
11. Puente, C.; Palacios, R.; González-Arechavala, Y.; Sánchez-Úbeda, E.F. Non-Intrusive Load Monitoring (NILM) for Energy Disaggregation Using Soft Computing Techniques. *Energies* **2020**, *13*, 3117. [\[CrossRef\]](#)
12. Li, C.; Zheng, K.; Guo, H.; Chen, Q. A mixed-integer programming approach for industrial non-intrusive load monitoring. *Appl. Energy* **2023**, *330*, 120295. [\[CrossRef\]](#)
13. Kalinke, F.; Bielski, P.; Singh, S.; Fouché, E.; Böhm, K. An Evaluation of NILM Approaches on Industrial Energy-Consumption Data. In *e-Energy '21, Proceedings of the Twelfth ACM International Conference on Future Energy Systems, Online, 28 June–2 July 2021*; Association for Computing Machinery: New York, NY, USA, 2021. [\[CrossRef\]](#)
14. Yuan, X.; Han, P.; Duan, Y.; Alden, R.E.; Rallabandi, V.; Ionel, D.M. Residential Electrical Load Monitoring and Modeling—State of the Art and Future Trends for Smart Homes and Grids. *Electr. Power Components Syst.* **2020**, *48*, 1125–1143. [\[CrossRef\]](#)
15. Nguyen, T.K.; Azarkh, I.; Nicolle, B.; Jacquemod, G.; Dekneuve, E. Applying NIALM technology to predictive maintenance for industrial machines. In Proceedings of the 2018 IEEE International Conference on Industrial Technology (ICIT), Lyon, France, 20–22 February 2018; pp. 341–345. [\[CrossRef\]](#)
16. Martins, P.B.M.; Gomes, J.G.R.C.; Nascimento, V.B.; de Freitas, A.R. Application of a Deep Learning Generative Model to Load Disaggregation for Industrial Machinery Power Consumption Monitoring. In Proceedings of the 2018 IEEE International Conference on Communications, Control, and Computing Technologies for Smart Grids (SmartGridComm), Aalborg, Denmark, 29–31 October 2018; pp. 1–6. [\[CrossRef\]](#)
17. Luan, W.; Yang, F.; Zhao, B.; Liu, B. Industrial load disaggregation based on Hidden Markov Models. *Electr. Power Syst. Res.* **2022**, *210*, 108086. [\[CrossRef\]](#)
18. Pan, J.; Li, C.; Tang, Y.; Li, W.; Li, X. Energy Consumption Prediction of a CNC Machining Process with Incomplete Data. *IEEE/CAA J. Autom. Sin.* **2021**, *8*, 987–1000. [\[CrossRef\]](#)
19. Meng, L.; Zhou, M.; Zhang, C.; Tian, G. A new model for predicting power consumption of machining processes: A turning case. In Proceedings of the 2016 IEEE International Conference on Automation Science and Engineering (CASE), Fort Worth, TX, USA, 21–25 August 2016; pp. 1289–1294. [\[CrossRef\]](#)
20. Cooper, D.R.; Rossie, K.E.; Gutowski, T.G. The energy requirements and environmental impacts of sheet metal forming: An analysis of five forming processes. *J. Mater. Process. Technol.* **2017**, *244*, 116–135. [\[CrossRef\]](#)
21. Gao, M.; He, K.; Li, L.; Wang, Q.; Liu, C. A Review on Energy Consumption, Energy Efficiency and Energy Saving of Metal Forming Processes from Different Hierarchies. *Processes* **2019**, *7*, 357. [\[CrossRef\]](#)
22. MathWorks. Deep Learning Toolbox: User's Guide. Available online: <https://es.mathworks.com/help/deeplearning/ref/neuralnetpatternrecognition-app.html> (accessed on 3 October 2023).
23. Zhang, G. Neural networks for classification: A survey. *IEEE Trans. Syst. Man Cybern. Part C (Applications Rev.)* **2000**, *30*, 451–462. [\[CrossRef\]](#)
24. Lin, H.-C.; Ye, Y.-C. Reviews of bearing vibration measurement using fast Fourier transform and enhanced fast Fourier transform algorithms. *Adv. Mech. Eng.* **2019**, *11*, 1687814018816751. [\[CrossRef\]](#)
25. Cabal-Yepez, E.; Garcia-Ramirez, A.G.; Romero-Troncoso, R.J.; Garcia-Perez, A.; Osornio-Rios, R.A. Reconfigurable monitoring system for time-frequency analysis on industrial equipment through STFT and DWT. *IEEE Trans. Ind. Inform.* **2013**, *9*, 760–771. [\[CrossRef\]](#)
26. Chang, H.-H.; Lian, K.-L.; Su, Y.-C.; Lee, W.-J. Power-Spectrum-Based Wavelet Transform for Nonintrusive Demand Monitoring and Load Identification. *IEEE Trans. Ind. Appl.* **2014**, *50*, 2081–2089. [\[CrossRef\]](#)
27. The MathWorks Inc. *Matlab*; The MathWorks Inc.: Natick, MA, USA, 2018.
28. Jain, V.K.; Collins, W.L.; Davis, D.C. High-Accuracy Analog Measurements via Interpolated FFT. *IEEE Trans. Instrum. Meas.* **1979**, *28*, 113–122. [\[CrossRef\]](#)

**Disclaimer/Publisher's Note:** The statements, opinions and data contained in all publications are solely those of the individual author(s) and contributor(s) and not of MDPI and/or the editor(s). MDPI and/or the editor(s) disclaim responsibility for any injury to people or property resulting from any ideas, methods, instructions or products referred to in the content.